Anticipatory synchronization with variable time delay and reset

G. Ambika*
Indian Institute of Science Education and Research, Pune 411 021, India

R. E. Amritkar†
Physical Research Laboratory, Ahmedabad 380 009, India

(Received 30 October 2008; revised manuscript received 17 February 2009; published 6 May 2009)

A method to synchronize two chaotic systems with anticipation or lag, coupled in the drive response mode, is proposed. The coupling involves variable delay with three time scales. The method has the advantage that synchronization is realized with intermittent information about the driving system at intervals fixed by a reset time. The stability of the synchronization manifold is analyzed with the resulting discrete error dynamics. The numerical calculations in standard systems such as the Rössler and Lorenz systems are used to demonstrate the method and the results of the analysis.

DOI: 10.1103/PhysRevE.79.056206 PACS number(s): 05.45.Xt, 05.45.Vx

I. INTRODUCTION

The synchronization of unidirectionally coupled chaotic systems has been studied reasonably well in the past few years [1–3]. The synchronization state in such cases can be phase, lag, generalized, or complete depending on the strength of the coupling [4,5]. Recently synchronization of systems via coupling with a time delay, which presumably takes care of the finite propagation times, switching speeds, and memory effects have been reported [6–9]. Such studies relate to a variety of diverse phenomena such as chirping of crickets, neural networks, automatic steering and control, and coupled phase-locked lasers [10–12]. When the coupling is not isochronous with the system dynamics, it is possible to realize retarded (delay), complete, and anticipatory synchronizations of chaotic systems. Moreover, synchronization in such cases reveals many novel phenomena such as parametric resonance [13], multistable phase clustering [14–17], amplitude death, etc. [18–20]. An interesting aspect of such a delay-induced synchronization, which has attracted a lot of attention, is that the driven system can anticipate the dynamics of the driver [21,22]. The maximum possible anticipation time is reported to be enhanced considerably by using an array or ring of such systems [23–25]. Experimental verification of anticipatory and retarded synchronizations is reported in electronic circuits as well as semiconductor lasers with delayed optoelectronic feedback [26,27]. In all these studies, the delay time in the coupling, once chosen, remains constant as the system evolves.

The synchronization of chaotic systems, in general, has attracted great attention due to its potential application in secure communication [28–30]. However the use of low-dimensional systems in this context is found to be insecure due to the ease of reconstruction from the transmitted signal [31,32]. Therefore, recently, chaos synchronization in high-dimensional systems, especially systems with an inherent time delay, has been proposed as a better alternative [33–37].

In this paper we propose a method of delay or anticipatory synchronization with coupling involving variable time delay. Here, the synchronization can be realized with limited information about the driver via occasional contacts or feedbacks at specific intervals. This makes the method highly cost effective and can be applied to cases where the signal transmission from the driver is slow or intermittent. This is achieved by using a variable delay in the coupling that is reset at definite intervals. The dynamics then evolves under three additional time scales, the delay τ_1, the anticipatory time τ_2, and the reset time τ. Unlike the case of fixed delay, the resetting mechanism makes the error dynamics discrete and it is possible to carry out an approximate analytic analysis. The analysis gives the maximum τ_2 for a given τ. This also fixes the regions of stability in the parameter plane of coupling and delay. The method is demonstrated for standard systems such as Rössler and Lorenz.

In addition to being novel, the method of anticipatory synchronization with variable delay and reset proposed here may be useful in secure communication. First, there are three time scales in the system which may lead to enhanced security. Second, the transmission load is less since the signal is needed only at the resetting time. This potential application and the likely benefits that may occur are further discussed in Sec. VI.

II. SYNCHRONIZATION WITH VARYING DELAY AND RESET

A. Model system

Consider a dynamical system x of dimension n that drives an identical system y. We choose a simple coupling term of the linear difference type but with the drive variable delayed by τ_1 and the driven variable delayed by τ_2. Thus, the dynamics is given by

$$\dot{x} = f(x), \tag{1a}$$

$$\dot{y} = f(y) + \epsilon \sum_{m=0}^{\infty} \Gamma(x_{t_1} - y_{t_2}) \chi_{(m\tau,(m+1)\tau)}, \tag{1b}$$

where $x_{t_1} = x(t-t_1)$, $y_{t_2} = y(t-t_2)$, τ is the resetting time, and $\chi_{(t',t'')}$ is an indicator function such that $\chi_{(t',t'')} = 1$ for $t' \leq t$

*g.ambika@iiserpune.ac.in
†amritkar@prl.res.in

$\leq t''$ and zero otherwise. Here, Γ is a matrix specifying the coupling between the components of x and y. For simplicity, we take Γ to be diagonal, $\Gamma=\text{diag}(\Gamma_1,\Gamma_2,\ldots,\Gamma_n)$, and in numerical simulations only one component Γ_i is assumed to be nonzero. Both the delays t_1 and t_2 depend on time and we choose this dependence as

$$t_i = \tau_i + t - m\tau, \quad i = 1,2.$$

Thus, $t-t_i=m\tau-\tau_i$ and this time dependence along with the indicator function ensure that $t_i \geq 0$. As the two systems evolve, t_1 and t_2 also evolve with the same time scale and the coupling term uses the same value of both variables x_{t_1} and y_{t_2} during each resetting time interval τ, i.e., the coupling term is constant for the time interval τ. In each time interval τ, the initial values of the delays t_1 and t_2 are τ_1 and τ_2, respectively. The delays increase linearly with time up to values $\tau_1+\tau$ and $\tau_2+\tau$ and then they are reset for the next interval. As a consequence, the coupling requires the variable of the drive system only at discrete time intervals of τ. We also note that $t_1-t_2=\tau_1-\tau_2$ for all t.

B. Synchronization manifold

Synchronization manifold for the coupled systems (1a) and (1b) is defined by $y(t-\tau_2)=x(t-\tau_1)$ or $y(t)=x(t-\tau_1+\tau_2)$. Thus, we can get all the following three possibilities [38]. (1) If $\tau_1-\tau_2>0$, we can get delay or lag synchronization with $\tau_1-\tau_2$ as the lag time. (2) If $\tau_1-\tau_2<0$, we can get anticipatory synchronization with $\tau_2-\tau_1$ as the anticipation time. (3) If $\tau_1-\tau_2=0$, we can get equal time synchronization.

As an illustration of this, we take the standard Rössler oscillator in the chaotic state as the driver described by the equations

$$\dot{x}_1 = -x_2 - x_3,$$

$$\dot{x}_2 = x_1 + ax_2,$$

$$\dot{x}_3 = b + x_3(x_1 - c). \tag{2}$$

This is coupled to an identical system through the coupling scheme given in Eq. (1). Only x_1 and y_1 are coupled, i.e., $\Gamma_1=1$ and $\Gamma_2=\Gamma_3=0$. Taking the parameter values $a=0.15$, $b=0.2$, and $c=10.0$, both systems are evolved from random initial conditions using Runge Kutta algorithm with a time step 0.01 for 2000 units of time. With $\tau=0.10$ and the coupling strength $\epsilon=0.4$, the resulting time series obtained for $\tau_1=0.84$ and $\tau_2=0.02$ is plotted in Fig. 1(a). Here the response system $y(t)$ (dashed line) lags behind the driver $x(t)$ (solid line) by $\tau_2-\tau_1$. Figure 1(b) shows the same for $\tau_1=0.02$ and $\tau_2=0.84$ where $y(t)$ anticipates $x(t)$ with the same time shift. The degree of synchronization with the corresponding time shift can be quantified using the similarity function defined as

$$S^2(T) = \frac{\langle [y_1(t) - x_1(t+T)]^2 \rangle}{\sqrt{\langle x_1^2(t)\rangle \langle y_1^2(t)\rangle}}. \tag{3}$$

Figures 1(c) and 1(d) show $S^2(T)$ computed for different values of T. The minimum occurs at 0.82, i.e., $T=|\tau_1-\tau_2|$, indicating synchronization with delay or anticipation of 0.82 time units.

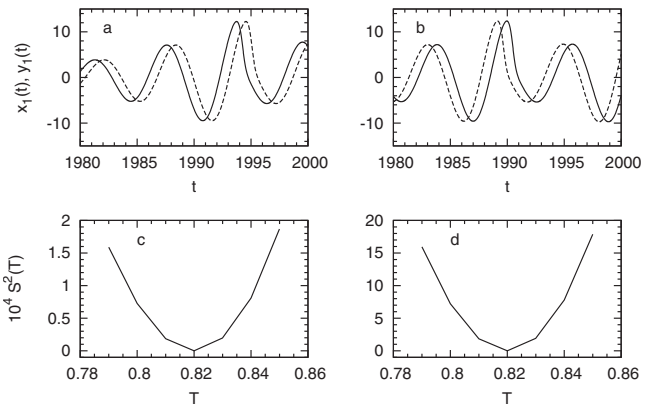

FIG. 1. The simulated time series of two Rössler systems coupled through the scheme in Eq. (1). In (a) the case of delay synchronization is shown with a delay of 0.82 units between the $x_1(t)$ (solid line) and $y_1(t)$ (dashed line). (b) is a case of anticipatory synchronization when $y_1(t)$ anticipates $x_1(t)$ by the same units. The similarity function $S^2(T)$ corresponding to both these cases are shown in (c) and (d), respectively.

It should be noted that the delay time τ_1 is not of much significance in the error dynamics, since the time scale of the drive system can be linearly shifted by τ_1. This point will become clear when we do the stability analysis in Sec. III.

III. LINEAR STABILITY ANALYSIS

The dynamics of the system in Eq. (1) involves three time scales in addition to its inherent scale. We define the transverse system by the variable $\Delta=y-x_{\tau_1-\tau_2}$. Its dynamics in linear approximation can be derived from Eq. (1) as

$$\dot{\Delta} = f'(x_{\tau_1-\tau_2})\Delta - \epsilon \sum_{m=0}^{\infty} \chi_{(m\tau,(m+1)\tau)}\Delta_m, \tag{4}$$

where $\Delta_m=\Delta(t-t_2)=\Delta(m\tau-\tau_2)$ and we take coupling in all components of x and y, i.e., $\Gamma_i=1$, $\forall i$. Thus, Δ_m is a constant in each time interval $m\tau \leq t < (m+1)\tau$. We note that τ_1 enters only through the Jacobian term f' and can be eliminated by shifting the time scale of the drive system linearly and redefining τ_2 suitably. Hence, as noted in Sec. II, τ_1 is not very significant for the stability analysis. The fixed point $\Delta=0$ corresponds to the lag or anticipatory synchronized state.

In general, it is not possible to solve Eq. (4). However, we can approximate the equation by replacing the Jacobian f' by some effective time average Lyapunov exponent λ (only the real part is required),

$$\dot{\Delta} = \lambda\Delta - \epsilon \sum_{m=0}^{\infty} \chi_{(m\tau,(m+1)\tau)}\Delta_m. \tag{5}$$

In the following analysis we assume λ to be positive. The results can be easily extended to $\lambda<0$ (see Appendix C).

From the numerical analysis presented in Sec. IV, it appears that the approximation of replacing f' by an effective λ

is reasonable for small values of τ_2. We need a larger value of λ for large τ_2.

In the interval $m\tau \le t < (m+1)\tau$, the solution of Eq. (5) is

$$\Delta = \alpha\Delta_m + C_m e^{\lambda t}, \tag{6}$$

where $\alpha = \epsilon/\lambda$ is the normalized dimensionless coupling constant and C_m is an integration constant.

A. $0 \le \tau_2 \le \tau$

Let us first consider the case $0 \le \tau_2 \le \tau$. For $t=(m+1)\tau - \tau_2$, $\Delta = \Delta_{m+1}$. Thus, eliminating the integration constant, Eq. (6), gives

$$\Delta = \alpha\Delta_m + (\Delta_{m+1} - \alpha\Delta_m)e^{\lambda[t-(m+1)\tau+\tau_2]}. \tag{7}$$

For $(m-1)\tau \le t \le m\tau$ we have

$$\Delta = \alpha\Delta_{m-1} + (\Delta_m - \alpha\Delta_{m-1})e^{\lambda(t-m\tau+\tau_2)}. \tag{8}$$

Matching solutions (7) and (8) at $t=m\tau$, and simplifying, we get the following recursion relation:

$$\Delta_{m+1} = \alpha\left(1 - e^{\lambda(\tau-\tau_2)} + \frac{1}{\alpha}e^{\lambda\tau}\right)\Delta_m - \alpha e^{\lambda\tau}(1 - e^{-\lambda\tau_2})\Delta_{m-1} \tag{9a}$$

$$= a\Delta_m - b\Delta_{m-1}, \tag{9b}$$

where

$$a = \alpha(1 - e^{\lambda(\tau-\tau_2)}) + e^{\lambda\tau}, \tag{10a}$$

$$b = \alpha e^{\lambda\tau}(1 - e^{-\lambda\tau_2}). \tag{10b}$$

We can write Eq. (9b) as a two-dimensional (2D) map in matrix form as

$$\begin{pmatrix} \Delta_{m+1} \\ \Delta_m \end{pmatrix} = \begin{pmatrix} a & -b \\ 1 & 0 \end{pmatrix}\begin{pmatrix} \Delta_m \\ \Delta_{m-1} \end{pmatrix}. \tag{11}$$

The eigenvalue equation for the Jacobian matrix is

$$\mu^2 - a\mu + b = 0, \tag{12}$$

with the solutions

$$\mu_\pm = \tfrac{1}{2}(a \pm \sqrt{a^2 - 4b}). \tag{13}$$

The synchronized state, $\Delta=0$, is stable if both the solutions satisfy $|\mu_\pm| < 1$. The detailed analysis of the stability conditions is given in Appendix A.

Figure 2 shows the stability region in the τ_2/τ-α plane. The lower limit of stability is always $\alpha_l = 1$. For smaller values of τ_2 ($\tau_2 \le \tau_{2p}$), the upper limit of stability is given by [Eq. (A6)]

$$\alpha_u = \frac{e^{\lambda\tau} + 1}{2e^{\lambda(\tau-\tau_2)} - e^{\lambda\tau} - 1}, \tag{14}$$

while for larger values of τ_2 ($\tau_{2p} \le \tau_2 \le \tau$) it is given by [Eq. (A8)]

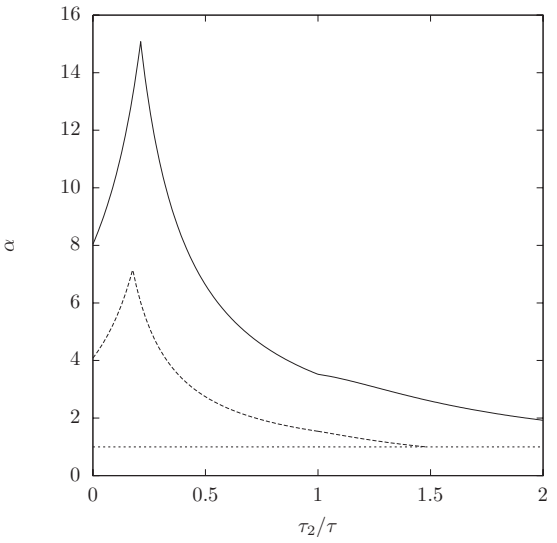

FIG. 2. This figure shows the stability region of the synchronized state [$\Delta=0$ solution of Eq. (9)] in the τ_2/τ-α plane. The solid line is for $\lambda\tau=0.25$ and the dashed line is for $\lambda\tau=0.5$. The lower limit of stability is $\alpha_l=1$ (dotted line). For smaller values of $\tau_2 \le \tau_{2p}$, the upper limit of stability is given by Eq. (14) while for larger values of τ_2 ($\tau_{2p} \le \tau_2 \le \tau$) it is given by Eq. (15). The peak values are (0.0530…/0.25…=0.212,15.083…) for $\lambda\tau=0.25$ and (0.088…/0.5=0.176…,7.169…) for $\lambda\tau=0.5$ [see Eqs. (16) and (17)]. For $\tau \le \tau_2 \le 2\tau$ the upper limit of stability is given by Eq. (27). The maximum value of $\lambda\tau_2$ is 0.74 for $\lambda\tau=0.5$.

$$\alpha_u = \frac{e^{-\lambda\tau}}{1 - e^{-\lambda\tau_2}}. \tag{15}$$

The maximum value of α_p is given by the intersection of the two curves (14) and (15),

$$\alpha_p = \frac{3 + e^{\lambda\tau}}{e^{\lambda\tau} - 1}. \tag{16}$$

The corresponding τ_{2p} value is given by

$$\tau_{2p} = \frac{\alpha_p(\alpha_p + 3)}{(\alpha_p + 1)^2}. \tag{17}$$

We also obtain $\tau_{2\max}$, the maximum allowed value of τ_2 for the stability of the synchronized state [Eq. (A9)]. A general expression for $\tau_{2\max}$ is obtained in Sec. III B [Eq. (29)].

B. $\tau_2 > \tau$

Let $\tau_2 = k\tau + \tau_2'$, $k=0,1,\ldots$, where $\tau_2' < \tau$. Consider solution (6) in the interval $m\tau \le t \le (m+1)\tau$. Then for $t=(m+1)\tau - \tau_2' = (m+k+1)\tau - \tau_2$, we get

$$\Delta_{m+k+1} = \alpha\Delta_m + C_m e^{\lambda(m+1)\tau - \lambda\tau_2'}. \tag{18}$$

Hence Eq. (6) becomes

$$\Delta = \alpha\Delta_m + (\Delta_{m+k+1} - \alpha\Delta_m)e^{\lambda[t-(m+1)\tau+\tau_2']}. \tag{19}$$

For $(m-1)\tau \le t \le m\tau$ we have

$$\Delta = \alpha\Delta_{m-1} + (\Delta_{m+k} - \alpha\Delta_{m-1})e^{\lambda(t-m\tau+\tau_2')}. \quad (20)$$

Equating solutions (19) and (20) for $t=m\tau$, and simplifying, we get the following recursion relation:

$$\Delta_{m+k+1} = e^{\lambda\tau}\Delta_{m+k} - \alpha(e^{\lambda(\tau-\tau_2')} - 1)\Delta_m - \alpha e^{\lambda\tau}(1 - e^{-\lambda\tau_2'})\Delta_{m-1}. \quad (21)$$

This gives a map of dimension $k+2$. In matrix form, the map can be expressed as

$$\begin{pmatrix} \Delta_{m+k+2} \\ \Delta_{m+k+1} \\ \Delta_{m+k} \\ \vdots \\ \Delta_m \end{pmatrix} = \begin{pmatrix} c & 0 & \dots & b_1 & b_0 \\ 1 & 0 & \dots & 0 & 0 \\ 0 & 1 & \dots & 0 & 0 \\ \vdots & & & & \vdots \\ 0 & 0 & \dots & 1 & 0 \end{pmatrix} \begin{pmatrix} \Delta_{m+k+1} \\ \Delta_{m+k} \\ \Delta_{m+k-1} \\ \vdots \\ \Delta_{m-1} \end{pmatrix}, \quad (22)$$

where $c=e^{\lambda\tau}$, $b_1=\alpha(e^{\lambda(\tau-\tau_2')}-1)$, and $b_0=\alpha e^{\lambda\tau}(1-e^{-\lambda\tau_2'})$. The eigenvalue equation is

$$\mu^{k+2} - c\mu^{k+1} + b_1\mu + b_0 = 0. \quad (23)$$

For $k=0$, the map of Eq. (22) reduces to the 2D map of Eq. (11). In general the behavior of the largest magnitude μ is as shown in Fig. 8(b), i.e., the stability range is from $\alpha_l=1$ until the complex μ has a magnitude of 1.

1. $k=1$, i.e., $\tau \le \tau_2 \le 2\tau$

For $k=1$, we have a three-dimensional (3D) map. The eigenvalue Eq. (23) becomes

$$\mu^3 - c\mu^2 + b_1\mu + b_0 = 0. \quad (24)$$

The lower stability limit is $\alpha_l=1$. The upper stability limit can be obtained by noticing that when the magnitude of the imaginary μ becomes 1, the two imaginary eigenvalues can be written as $\mu=e^{\pm i\theta}$ and the above equation has a factor $\mu^2-2\cos(\theta)\mu+1$. This gives the condition

$$b_0^2 + cb_0 + b_1 - 1 = 0. \quad (25)$$

Using this we get a quadratic equation for α,

$$a_2\alpha^2 + a_1\alpha - 1 = 0, \quad (26)$$

where $a_1=e^{2\lambda\tau}(1-e^{-\lambda\tau_2'})+e^{\lambda(\tau-\tau_2')}-1$ and $a_2=e^{2\lambda\tau}(1-e^{-\lambda\tau_2'})^2$. One solution of this equation gives the upper stability limit for α,

$$\alpha_u = \frac{1}{2a_2}(-a_1 + \sqrt{a_1^2 + 4a_2}). \quad (27)$$

This upper stability limit is shown in Fig. 2 for $\tau \le \tau_2 \le 2\tau$.

We can also obtain $\tau_{2\max}'$, the maximum value of τ_2' for which synchronization is possible. This happens when there is always an eigenvalue with magnitude greater than 1, i.e., when $\alpha_l=\alpha_u=1$. By setting $\alpha_u=\alpha_l=1$ in Eq. (26), we get $a_1+a_2=1$. However a better condition is obtained if we note that for $\alpha_u=\alpha_l=1$, Eq. (24) has two degenerate solutions $\mu=1$, i.e., Eq. (24) has a factor $\mu^2-2\mu+1$. This gives the conditions $b_0=2-c$ and $1-b_1=2(2-c)$. First condition gives

$$\lambda\tau_{2\max} = \lambda\tau + \lambda\tau_{2\max}' = \lambda\tau - \ln 2 - \ln(1 - e^{-\lambda\tau}). \quad (28)$$

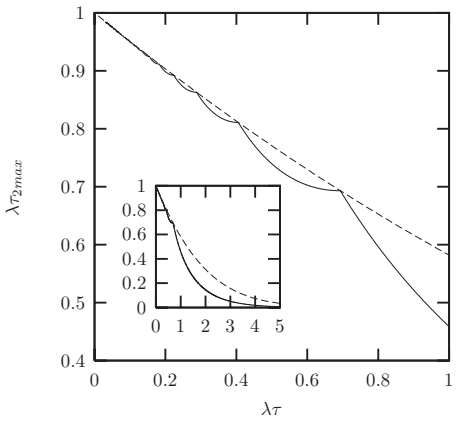

FIG. 3. The figure plots the maximum $\tau_{2\max}$ as a function of $\lambda\tau$ (solid line). Here, $\tau_{2\max}$, $k=0,1,2,\ldots$, is given by Eq. (29) and for each k the range of τ is (τ_k,τ_{k+1}). The dashed curve passes through the values $\tau_{2\max}=k\tau_k=k\ln((k+1)/k)$ [Eq. (30)]. The inset shows the same plot with $\lambda\tau$ range (0,5).

2. General k

For a general k, getting explicit solutions for α_u is not easy. But it is possible to get an expression for $\tau_{2\max}'$. We use the condition that for $\alpha_u=\alpha_l=1$, Eq. (23) has two degenerate solutions $\mu=1$. This gives the condition $b_0=1+k-kc$. Simplifying, we get

$$\lambda\tau_{2\max} = k\lambda\tau + \lambda\tau_{2\max}' = k\lambda\tau - \ln(k+1) - \ln(1 - e^{-\lambda\tau}). \quad (29)$$

For $k=0$, this equation reduces to Eq. (A9) and for $k=1$ it reduces to Eq. (28). Figure 3 shows the plot of $\lambda\tau_{2\max}$ as a function of τ for different k values. For each k the plot is for the range (τ_k,τ_{k+1}) where τ_k is defined by $k\tau_k=\tau_{2\max}$ and from Eq. (29) we get $\tau_k=\ln((k+1)/k)$.

3. $\tau_2=n\tau$

In this case it is not possible to obtain the stability range for the synchronized state in terms of α. However, it is possible to obtain an explicit expression for $\tau_{2\max}$ as (the detailed calculations are given in Appendix B)

$$\lambda\tau_{2\max} = \lambda\tau/[\exp(\lambda\tau) - 1]. \quad (30)$$

The dashed line in Fig. 3 corresponds to Eq. (30). It gives the correct $\tau_{2\max}$ only for $\tau_2=n\tau$.

IV. LYAPUNOV EXPONENTS

Since we have several time scales, one has to be careful in calculating the Lyapunov exponents. We adapt the procedure introduced by Farmer [39] and discretize at intervals, h,

where h is the time step of the integration. For these calculations we choose $\tau_1=0$ and first consider the case $0\leq\tau_2<\tau$. Since we have a variable time delay, the procedure of Farmer [39] needs a modification. We introduce the discrete difference vector, $\zeta(k)$, according to the time scale τ and it is defined by

$$\zeta(k) = \{\Delta[(k-1)\tau+h], \Delta[(k-1)\tau+2h], \ldots, \Delta(k\tau)\} = (\zeta_1, \zeta_2, \ldots, \zeta_N), \tag{31}$$

where $N=\tau/h$. Since Δ is n dimensional, ζ is nN dimensional. Here, k is the time index. The vector ζ evolves according to Eq. (4) and therefore the vector $\zeta(k+1)$ is obtained from $\zeta(k)$ as follows:

$$\zeta_1(k+1) = \zeta_N(k) + \{f'[x(k\tau+\tau_2)]\zeta_N(k) - \epsilon\zeta_{N-j}(k)\}h,$$

$$\zeta_2(k+1) = \zeta_1(k+1) + \{f'[x(k\tau+\tau_2+h)]\zeta_1(k+1) - \epsilon\zeta_{N-j}(k)\}h,$$

$$\vdots$$

$$\zeta_N(k+1) = \zeta_{N-1}(k+1) + (f'\{x[k\tau+\tau_2+(N-1)h]\} \times\zeta_{N-1}(k+1) - \epsilon\zeta_{N-j}(k))h, \tag{32}$$

where $j=\tau_2/h$. Each time step k to $k+1$ advances the time by τ. To obtain the transverse Lyapunov exponents, one starts with a set of orthonormal vectors $\zeta^{(i)}(0)$, with $i=1,2,\ldots$ as initial conditions and evolve them according to the above equations and orthonormalize them at each step. The i th Lyapunov exponent is then given by $\lim_{T\to\infty}(1/(T\tau))\Sigma_{k=1}^{T}\ln(a_i(k))$, where a_i is the normalization factor for the ith vector. In our case this procedure can yield only $n+l$ transverse Lyapunov exponents where l is the number of nonzero elements in the diagonal matrix Γ, indicating that the dimension of our coupled system is $2n+l$.

For $\tau_2\geq\tau$, it is necessary to define higher-dimensional vectors, e.g., when $\tau\leq\tau_2<2\tau$, the discretization is to be done over the interval 2τ, and hence the dimension of the difference vector ζ must be $2nN$. The equations for the general case are included in Appendix D.

V. NUMERICAL ANALYSIS

We choose two standard systems, Rössler and Lorenz, to confirm the main results obtained in Secs. III and IV. In the case of Rössler system given in Eq. (2), two identical systems are coupled in the drive response mode via the coupling scheme explained in Eq. (1). Starting from random initial conditions and choosing the system parameters in the chaotic region ($a=0.15$, $b=0.2$, and $c=10.0$), they are evolved for 200 000 units with a time step of 0.01. The correlation coefficient $C=\langle y_1(t)x_1(t+\tau_2)\rangle/\sqrt{\langle x_1^2(t)\rangle\langle y_1^2(t)\rangle}$ between $x_1(t)$ and $y_1(t)$ shifted by the effective $\tau_2=|\tau_2-\tau_1|$ (hereafter referred to as τ_2 itself) is calculated using the last 5000 values. The region of stability of the synchronized state is isolated as the region where $C=0.99$ and boundaries of stability fixed when C goes below this value.

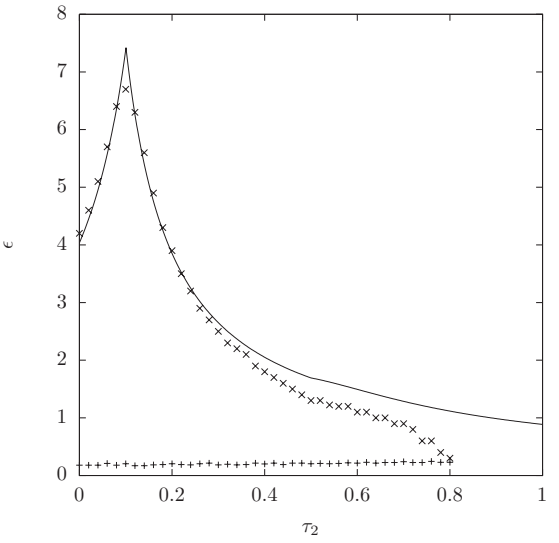

FIG. 4. The limits of stability of the synchronized state of two chaotic Rössler systems in the parameter plane τ_2-ϵ. The solid line is the limits obtained from the stability analysis for $\lambda=0.65$. The agreement is good for values of $\epsilon>3.0$.

Taking $\tau=0.5$, τ_2 is varied from 0 to 1.0 units in steps of 0.01. For each value of τ_2, the coupling strength ϵ is increased in steps of 0.005. The appropriately shifted correlation coefficient is calculated and using the criterion mentioned above, the lower and upper limits of stability are found out. The results are plotted in the parameter plane τ_2-ϵ in Fig. 4. The overall behavior agrees with the theoretical analysis carried out in Sec. IV. The upper limits obtained by the stability analysis given in Eqs. (14), (15), and (27) for the different relative ranges of τ_2 are calculated for a typical value of $\lambda=0.65$ and shown as a solid line. For values of $\tau_2<0.3$ or $\epsilon>3.0$, the agreement is good although for lower values, there is deviation. For lower values of ϵ we need larger values of λ to obtain a better fit (not shown in the figure).

By fixing the coupling $\epsilon=0.8$, we vary the reset time τ in the range (0,2.0) in steps of 0.01 and in each case the maximum value of τ_2 for the stability of synchronization is calculated using the same criterion. The results are shown in Fig. 5. The $\tau_{2\max}$ obtained from theory and shown in Fig. 3 are reproduced here for comparison. The numerical values are found to support the results of the theoretical analysis very well. We note that here the λ dependence cancels out, and hence the agreement with the theory is much better than that for the τ_2-ϵ plots.

Using the procedure described in Sec. IV, we compute the Largest Transverse Lyapunov Exponent (LTLE) for the range of ϵ values (0.1,8.0) and τ_2 in the range (0,0.8) with $\tau=0.5$.

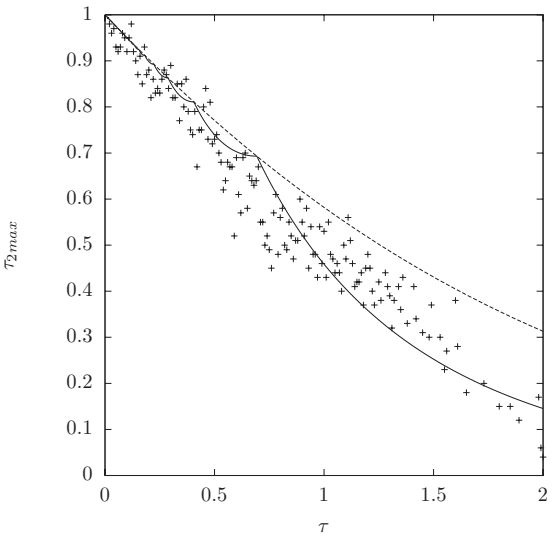

FIG. 5. The maximum values of τ_2 for which anticipatory synchronization is stable in two coupled Rössler systems is shown as a function of the reset time τ. The solid and dotted lines are the similar values from theory reproduced from Fig. 3 for comparison.

The contour plot of the LTLE values is shown in Fig. 6. The stability curves in Fig. 4 obtained by calculating the correlation is found to be in reasonable agreement with the zero contour of LTLE (see Figs. 4 and 6).

We consider next two Lorenz systems, where the x system is given by

$$\dot{x}_1 = a(x_2 - x_1),$$

$$\dot{x}_2 = cx_1 - x_2 - x_1x_3,$$

$$\dot{x}_3 = -bx_3 + x_1x_2. \tag{33}$$

This is coupled to an identical y system using the same

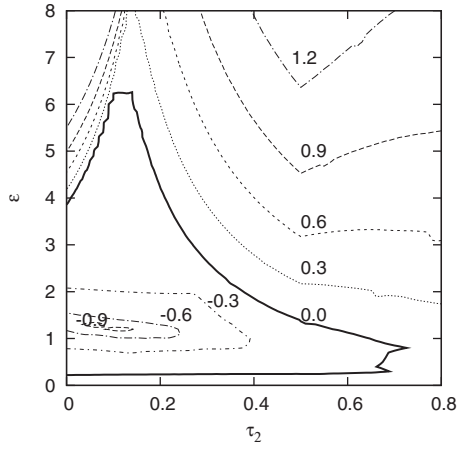

FIG. 6. The contour of the largest Transverse Lyapunov Exponent (LTLE) values of two coupled Rössler systems. The ranges of parameters are the same as in Fig. 4. The contours shown are for (−0.9,1.2) in steps of 0.3. The contour of zero LTLE agrees well with the stability curves obtained from correlations, shown in Fig. 4.

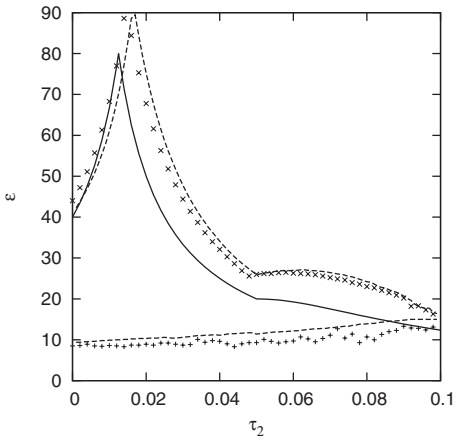

FIG. 7. The critical values of coupling ϵ for two coupled Lorenz systems as a function of the anticipatory time τ_2 for stability. The solid curve is the limiting curve from theory that is the same as in Fig. 2 for a value of $\lambda=0.0$. The dotted line is the limits of stability obtained from zero crossing of largest transverse Lyapunov exponent values while the crosses give stability limits from correlation criterion.

scheme. Choosing parameter values for chaotic Lorenz as $a=10.0$, $b=8/3$, and $c=28.0$, the analysis is repeated as in the case of Rössler. Here the time step chosen is 0.001 and $\tau=0.05$. The τ_2 values are varied in the range (0,0.1) and the stability limits of ϵ isolated using the criterion, correlation $C=0.99$ for stability. For the same range of parameters, we compute the LTLE and its zero crossing is taken as the limit of stability. Both these results are given in the same figure, Fig. 7, along with the curves of stability from theory for $\lambda=0.0$ (solid line). The dotted lines indicate the values for zero LTLE and the crosses denote the stability limits obtained from correlation analysis.

VI. CONCLUSION

We introduce a coupling scheme with varying time delay for synchronization of two systems with delay or anticipation. The scheme has the advantage that synchronization can be achieved with intermittent information from the driver in intervals of reset that can be prefixed. This also makes a detailed stability analysis analytically possible because the error dynamics becomes discrete. By assuming an average effective Lyapunov exponent λ, the stability regions and limits of stability in the parameters of coupling strength and anticipation time are worked out for specific cases. We demonstrate the method by numerical simulations in two standard systems, Rössler and Lorenz. The general features of the stability region in parameter space match with the theoretical stability analysis, but more precise matching with the numerical data is not possible. This is understandable since in the analytical calculations f' is replaced by an effective λ and also coupling in all components of x and y is assumed

while in numerical calculations only one component is coupled. The agreement between the theory and numerical data is reasonably good for the $\tau_{2\max}$-τ plot, since the λ dependence cancels out. The scheme for computation of the transverse Lyapunov exponents for this type of coupling is presented and tried out for both Rössler and Lorenz systems. The range of stability based on this is found to agree well with that obtained from the numerical calculations based on correlations.

The availability of three time scales in the dynamics is suggestive of potent applications especially in secure communication. We propose that this technique will be especially successful with a bichannel transmission [40] where one channel, which is part of the state space of the chaotic transmitter (driver), is used to synchronize with the receiver (response) and the other forms the message along with the chaotic signal from a different part of the state space of the driver. Here since the encrypted information or cipher text is not used as the synchronizing signal, it can be made really complex and secure. In this context our method of synchronization has the definite advantage that the synchronization channel needs to be transmitted only at intervals fixed by the reset time which itself forms part of the key space. Less amount of transmission leads to less load on the channel, bandwidth savings, and requirement of noise-free channel for short times. Moreover, the enhancement in the dimensionality of the key space and also less amount of transmitted signal can lead to an increase in security. The stability analysis reported in this paper along with the numerical simulations for standard systems helps one to fix the accessible regions of the key space for better key management. This is being worked out and will be published elsewhere.

ACKNOWLEDGMENTS

One of the authors, G.A., acknowledges the hospitality and facilities at Physical Research Laboratory, Ahmedabad.

APPENDIX A: CASE $0 \leq \tau_2 \leq \tau$

Here we analyze the eigenvalues $\mu_\pm$ of map (11) given by Eq. (13) to obtain the stability conditions. These stability conditions are shown in Fig. 2. The synchronized state, $\Delta = 0$, is stable if both the eigenvalues satisfy $|\mu_\pm| < 1$.

1. $\tau_2 = 0$

For this case $b=0$. Hence, the 2D map in Eq. (11) becomes a one-dimensional (1D) map given by

$$\Delta_{m+1} = \mu \Delta_m, \tag{A1}$$

where $\mu = \alpha[1-(1-\frac{1}{\alpha})e^{\lambda\tau}]$. Figure 8(a) shows μ as a function of $1/\alpha$. The fixed point $\Delta=0$ is stable provided that $|\mu|<1$.

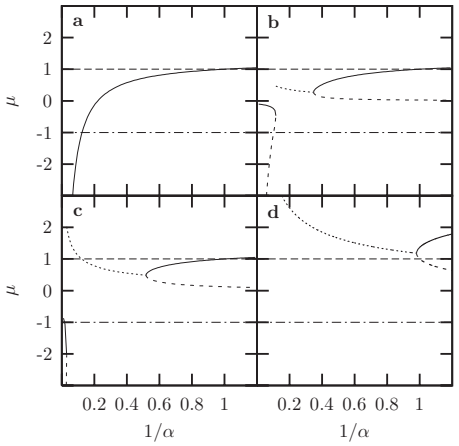

FIG. 8. This figure shows the eigenvalues μ as a function of $1/\alpha$. (a) $\lambda\tau=0.25$ and $\lambda\tau_2=0$. Here, $\mu=\alpha[1-(1-\frac{1}{\alpha})e^{\lambda\tau}]$ [see Eq. (A1)]. (b) $\lambda\tau=0.25$ and $\lambda\tau_2=0.02$. The largest μ (solid line) starts from a value greater than 1 for $1/\alpha>1$, crosses 1 at $1/\alpha=1$, and continues until it meets the dashed line from below (here $a^2-4b=0$). Then μ becomes complex and the dotted line shows the magnitude $|\mu|$. This continues until we have $a^2-4b=0$ again. This point is just above the meeting point of solid and dashed lines on the negative side. For smaller values of $1/\alpha$, μ again become real (but now negative) and the largest μ in magnitude jumps to the dashed line bellow. Hence the stability range is from $\alpha=1$ until the point where $\mu=-1$. (c) $\lambda\tau=0.25$ and $\lambda\tau_2=0.1$. This figure is similar to (b), but here the dotted line (μ complex) crosses the magnitude one before jumping to the negative value. Hence the stability range is now from $\alpha=1$ until the point where the dotted line crosses one or the complex μ has a magnitude of 1. Crossover from the behavior (b) to (c) occurs at the peak value, α_p, as seen in Fig. 2. (d) $\lambda\tau=1.0$ and $\lambda\tau_2=0.7$. Here, $\tau_2>\tau_{2\max}=0.458\ldots$. Hence, the largest $|\mu|$ is always greater than 1.

This gives the following limits on α for the stability of the synchronized state:

$$1 < \alpha < \frac{1+e^{-\lambda\tau}}{1-e^{-\lambda\tau}}. \tag{A2}$$

2. $0 < \tau_2 < \tau$

For $0<\tau_2<\tau$, the eigenvalues $\mu_\pm$ [Eq. (13)] display a rich behavior. Three different scenarios are possible. These are shown in Figs. 8(b)–8(d) which show μ as a function of $1/\alpha$. To determine the limits of stability of the solution $\Delta=0$ we consider the following cases.

a. $\mu=1$ $(a^2-4b>0, a>0)$

Setting $\mu=1$ in Eq. (13), we get $2=a\pm\sqrt{a^2-4b}$. This reduces to

$$1 = a - b. \tag{A3}$$

Using expressions (10a) and (10b) for a and b, we get the

lower limit on the stability as

$$\alpha_l = 1. \tag{A4}$$

b. $\mu=-1$ ($a^2-4b>0, a<0$)

Setting $\mu=-1$ in Eq. (13), we get $-2=a\pm\sqrt{a^2-4b}$ which reduces to

$$1 + a + b = 0. \tag{A5}$$

Using expressions (10a) and (10b), we get

$$\alpha_u = \frac{e^{\lambda\tau}+1}{2e^{\lambda(\tau-\tau_2)} - e^{\lambda\tau} - 1}. \tag{A6}$$

The above expression gives the upper limit of stability for smaller values of τ_2. For larger values of τ_2, we use the condition $|\mu|=1$ which is considered in Appendix A 2 c.

c. $|\mu|=1$ ($a^2-4b<0$, μ is complex)

Setting $|\mu|=1$ (μ is complex) in Eq. (13), we get $1=\frac{1}{2}\sqrt{a^2-(a^2-4b)}$ which reduces to

$$b = 1. \tag{A7}$$

Substituting from Eq. (10b), we get the upper limit on the stability as

$$\alpha_u = \frac{e^{-\lambda\tau}}{1 - e^{-\lambda\tau_2}}. \tag{A8}$$

The above expression can also be used to determine the maximum $\tau_{2\max}$ for a given τ. This happens when there is always an eigenvalue with magnitude greater than 1, i.e., when $\alpha_l=\alpha_u=1$. From Eq. (A8) we get the following expression:

$$\lambda\tau_{2\max} = -\ln(1 - e^{-\lambda\tau}). \tag{A9}$$

Note that $\alpha_u=1$ in Eq. (A6) gives the same $\tau_{2\max}$ as in Eq. (A9). Figure 8(d) shows μ as a function of $1/\alpha$ for $\tau_2 > \tau_{2\max}$ where the synchronized state is not stable.

d. Peak

The peak value α_p is given by the intersection of Eqs. (A6) and (A8) and leads to the conditions

$$b = 1 \quad \text{and} \quad a + 2 = 0. \tag{A10}$$

From $b=1$, we have

$$e^{-\lambda\tau_2} = 1 - \frac{1}{\alpha}e^{-\lambda\tau}. \tag{A11}$$

Substituting this in $a+2=0$, we get

$$\alpha_p = \frac{e^{\lambda\tau}+3}{e^{\lambda\tau}-1}. \tag{A12}$$

The corresponding τ_2 value is given by

$$\lambda\tau_{2p} = \lambda\tau + \ln(e^{\lambda\tau}+3) - 2\ln(e^{\lambda\tau}+1). \tag{A13}$$

Eliminating τ from Eqs. (A12) and (A13) gives Eq. (17).

3. $\tau_2=\tau$

This is a simple case where a and b in Eqs. (10a) and (10b) reduce to $a=c=e^{\lambda\tau}$, $b=d=\alpha(e^{\lambda\tau}-1)$. The cases in Appendix A 2 a and A 2 c are applicable, and hence the stability condition for $\Delta=0$ is

$$1 < \alpha < \frac{1}{e^{\lambda\tau}-1}. \tag{A14}$$

APPENDIX B: CASE $\tau_2=n\tau$

This corresponds to the case $\tau_2'=0$ in Sec. III B. Using Eq. (21), we get the following recursion relation (note that $n=k+1$ gives the correct correspondence):

$$\Delta_{m+n+1} = e^{\lambda\tau}\Delta_{m+n} - \alpha(e^{\lambda\tau}-1)\Delta_m \tag{B1a}$$

$$= c\Delta_{m+n} - d\Delta_m, \tag{B1b}$$

where $c=e^{\lambda\tau}$ and $d=\alpha(e^{\lambda\tau}-1)$. This leads to an $(n+1)$-dimensional map. This map can also be obtained directly from solution (6) noting that for $t=m\tau$ and $t=(m+1)\tau$ we get Δ_{m+n} and Δ_{m+n+1}, respectively. In matrix form

$$\begin{pmatrix} \Delta_{n+1} \\ \Delta_n \\ \Delta_{n-1} \\ \vdots \\ \Delta_1 \end{pmatrix} = \begin{pmatrix} c & 0 & \cdots & 0 & -d \\ 1 & 0 & \cdots & 0 & 0 \\ 0 & 1 & \cdots & 0 & 0 \\ \vdots & \vdots & \vdots & \vdots & \vdots \\ 0 & 0 & \cdots & 1 & 0 \end{pmatrix} \begin{pmatrix} \Delta_n \\ \Delta_{n-1} \\ \Delta_{n-2} \\ \vdots \\ \Delta_0 \end{pmatrix}. \tag{B2}$$

The eigenvalue equation is

$$\mu^{n+1} - c\mu^n + d = 0, \tag{B3}$$

where $n \geq 1$.

The following general conclusions can be arrived by using Geršgorin disks. There is one disk with its center at c and radius d and n disks with their center at 0 and radius 1. All the eigenvalues lie within these disks. For $\alpha<1$, $c>d+1$. Hence, the disk with its center at c is disjoint from the other disks. Thus one root which lies in this disk must always have a magnitude greater than 1. Hence, the lower limit of stability is $\alpha_l=1$.

For $n=1$, Eq. (B3) becomes a quadratic equation. This is discussed in Appendix A 3.

1. $n=2$

Equation (B3) becomes a cubic equation,

$$\mu^3 - c\mu^2 + d = 0. \tag{B4}$$

At the upper stability limit, μ is complex with $|\mu|=1$. Thus, $\mu^2-2\cos(\theta)\mu+1$ is a factor where $\mu=e^{\pm i\theta}$. Using this condition we get the relation

$$d^2 + cd = 1. \tag{B5}$$

This gives a quadratic equation in α,

$$(e^{\lambda\tau}-1)^2\alpha^2 + e^{\lambda\tau}(e^{\lambda\tau}-1)\alpha - 1 = 0. \tag{B6}$$

Using the correct solution the stability range is

$$1 < \alpha < \frac{1}{2(e^{\lambda\tau}-1)}(\sqrt{e^{2\lambda\tau}+4} - e^{\lambda\tau}). \tag{B7}$$

The maximum $\tau_{2\max}$ is obtained in Appendix B 2.

2. Any n

For a general n it is not possible to obtain the stability range for the synchronized solution. It is easy to see that the maximum $\tau_{2\max}$ is obtained if there are two degenerate eigenvalues of Eq. (B3) equal to 1 at $\alpha=1$. This is possible if $c=1/n$, $d=1+1/n$. Using the explicit form of c or d and $n=\tau_{2\max}/\tau$, we get Eq. (30) for $\tau_{2\max}$.

APPENDIX C: NEGATIVE λ

If the Lyapunov exponent λ is negative, then Eq. (5) can be written as

$$\dot{\Delta} = -|\lambda|\Delta - \epsilon\sum_{m=0}^{\infty}\chi_{(m\tau,(m+1)\tau)}\Delta_m. \tag{C1}$$

The analysis is similar to that for positive λ. Here, we summarize the results.

1. $0 \le \tau_2 \le \tau$

For $0 \le \tau_2 \le \tau$, Eq. (C1) leads to the recursion relation [see Eq. (9)]

$$\Delta_{m+1} = a\Delta_m - b\Delta_{m-1}, \tag{C2}$$

where

$$a = -\alpha(e^{|\lambda|(\tau_2-\tau)} - 1) + e^{-|\lambda|\tau}, \tag{C3a}$$

$$b = \alpha e^{-|\lambda|\tau}(e^{|\lambda|\tau_2} - 1), \tag{C3b}$$

where we define $\alpha=\epsilon/|\lambda|$ as the normalized dimensionless coupling constant.

a. $\tau_2=0$

For $\tau_2=0$, $b=0$. The stability limits for the synchronized state are [see Eq. (A2)]

$$-1 < \alpha < \frac{1+e^{-|\lambda|\tau}}{1-e^{-|\lambda|\tau}}. \tag{C4}$$

b. $0 < \tau_2 \le \tau$

In this case Eq. (C2) leads to a 2D map as for the positive λ. The eigenvalue equation and the solutions are the same as Eqs. (12) and (13) with a and b defined by Eqs. (C3a) and (C3b).

The lower stability limit is always $\alpha_l=-1$. For smaller values of τ_2 ($\le\tau_{2p}$), the upper limit of stability is given by [see Eq. (14)]

$$\alpha_u = \frac{1+e^{-|\lambda|\tau}}{1+e^{-|\lambda|\tau}-2e^{|\lambda|(\tau_2-\tau)}}, \tag{C5}$$

while for larger values of τ_2 ($\tau_{2p} \le \tau_2 \le \tau$) it is given by [Eq. (15)]

$$\alpha_u = \frac{e^{|\lambda|\tau}}{e^{|\lambda|\tau_2}-1}. \tag{C6}$$

It is interesting to note that for very large values of the coupling constant, the synchronized state is unstable. The maximum value of α_p is given by the intersection of the two curves (C5) and (C6),

$$\alpha_p = \frac{3e^{\lambda\tau}+1}{e^{\lambda\tau}-1}. \tag{C7}$$

The corresponding τ_{2p} value is determined by the relation

$$|\lambda|\tau_{2p} = |\lambda|\tau + 2\ln(1+e^{-|\lambda|\tau}) - \ln(3+e^{-|\lambda|\tau}). \tag{C8}$$

c. $\tau_2=\tau$

For $\tau_2=\tau$, the stability range is

$$-1 < \alpha < \frac{1}{1-e^{-|\lambda|\tau}}. \tag{C9}$$

2. $\tau_2 > \tau$

Let $\tau_2=k\tau+\tau_2'$, $k=0,1,\ldots$, where $\tau_2'<\tau$ as for the case of positive λ. Equation (C1) leads to a map of dimension $k+2$. The eigenvalue equation is

$$\mu^{k+2} - c\mu^{k+1} + b_1\mu + b_0 = 0, \tag{C10}$$

where $c=e^{-|\lambda|\tau}$, $b_1=\alpha(1-e^{|\lambda|(\tau_2'-\tau)})$, and $b_0=\alpha e^{-|\lambda|\tau}(e^{|\lambda|\tau_2'}-1)$. For $k=0$, we recover the case $0<\tau_2\le\tau$.

For $k=1$, i.e., $\tau\le\tau_2\le 2\tau$, we have a 3D map. The lower stability limit is $\alpha_l=-1$. The upper stability limit is

$$\alpha_u = \frac{1}{2a_2}(a_1 + \sqrt{a_1^2+4a_2}), \tag{C11}$$

where $a_1=e^{-2|\lambda|\tau}(1-e^{|\lambda|\tau_2'})+e^{|\lambda|(\tau_2'-\tau)}-1$ and $a_2=e^{-2|\lambda|\tau}(e^{|\lambda|\tau_2'}-1)^2$. The stability limits are plotted in Fig. 9.

We have done numerical analysis for negative λ using two Rössler systems in the periodic region for $c=2.2$. The stability limits for synchronization in the τ_2-ϵ plane in this case is given in Fig. 10. The solid line is the curve from theory with $\lambda=0.0$. The behavior of the numerical results in general agrees with the theoretical analysis. However, exact

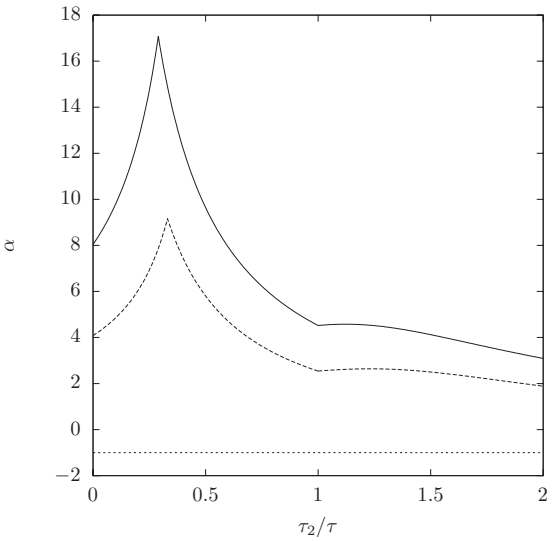

FIG. 9. The stability region of the synchronized state in the $|\lambda|\tau_2$-α plane. The solid line is for $\lambda\tau=-0.25<0$ and the dashed line is for $\lambda\tau=-0.5$. The lower limit of stability is $\alpha_l=-1$ (dotted line). For smaller values of $\tau_2 \leq \tau_{2p}$, the upper limit of stability is given by Eq. (C5) while for larger values of τ_2 ($\tau_{2p} \leq \tau_2 \leq \tau$) it is given by Eq. (C6). The peak values are (0.072…/0.25… =0.29,17.083…) for $\lambda\tau=-0.25$ and (0.165…/0.5 =0.33…,9.16…) for $\lambda\tau=-0.5$ [see Eqs. (C7) and (C8)]. For $\tau \leq \tau_2 \leq 2\tau$ the upper limit of stability is given by Eq. (C11). We note that the stability limits have a similar behavior to that of Fig. 2 for positive λ.

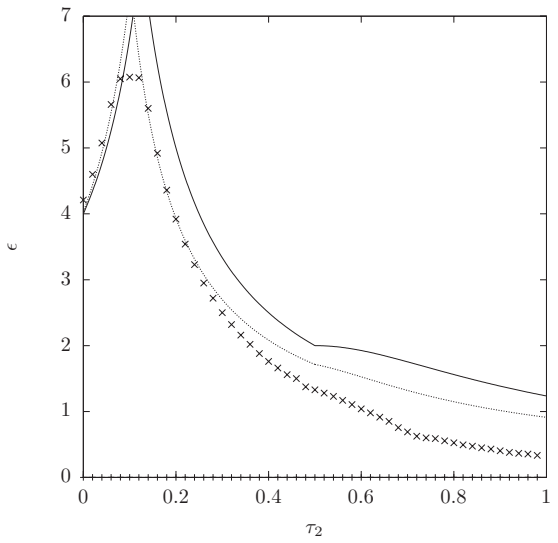

FIG. 10. The maximum values of coupling ϵ for two coupled Rössler systems in the periodic region. The solid curve is for the values from theory reproduced from Fig. 9 for a value of $\lambda=0.0$. The agreement is better with the curves in Fig. 2 (dotted line) for a value of $\lambda=0.6$.

fit is not obtained for any negative λ. Surprisingly, the fit is better for positive λ with equations Eqs. (14) and (15) (dotted line). The reason for this behavior is not clear.

3. $\tau_{2\max}$

The condition for obtaining the maximum value $\tau_{2\max}$ is that $\alpha_l=\alpha_u$. For negative λ, we have $\alpha_l=-1$ and α_u always remains positive. Hence, unlike the case of positive λ, the condition for obtaining $\tau_{2\max}$ is never satisfied and synchronized state is possible for any τ_2 or $\tau_{2\max}$ that is infinite.

4. $\tau_2=n\tau$

This corresponds to the case $\tau_2'=0$ of Appendix C 2. The eigenvalue equation is [see Eq. (B3)]

$$\mu^{n+1} - c\mu^n + d = 0, \tag{C12}$$

where $n \geq 1$ and $c=e^{-|\lambda|\tau}$ and $d=\alpha(1-e^{-|\lambda|\tau})$.

The following general conclusions can be arrived at using the Geršgorin disks. There is one disk with its center at c and radius $|d|$ and n disks with its center at 0 and radius 1. All the eigenvalues lie within these disks. For $\alpha<1$, $d<(1-c)$. Since $c<1$, the disk with its center at c lies within the circle $|\mu|=1$. Hence, all the roots of Eq. (C12) have magnitude less than 1 and the synchronized state is stable. Thus for any n there will be range of α values for which the synchronized state is stable. This supports the conclusion reached in Appendix C 3 that $\tau_{2\max}$ is infinite.

For $n=1$, Eq. (C12) becomes a quadratic equation. This is discussed in Appendix C 1.

For $n=2$ we have a cubic equation. The stability range is

$$-1 < \alpha < \frac{1}{2(1-e^{-|\lambda|\tau})}(\sqrt{e^{-2|\lambda|\tau}+4} - e^{-|\lambda|\tau}). \tag{C13}$$

APPENDIX D: COMPUTATION OF LYAPUNOV EXPONENTS

Here we give the scheme for calculating the Lyapunov exponents for the general case when $(m-1)\tau \leq \tau_2 < m\tau$. Let $N=\tau/h$ and $j=\tau_2/h$. We consider the discrete difference vector

$$\begin{aligned}\zeta(k) = \{&\Delta[(mk-m)\tau+h], \Delta[(mk-m)\tau+2h], \ldots,\\ &\Delta[(mk-m+1)\tau],\\ &\Delta[(mk-m+1)\tau+h],\\ &\Delta[(mk-m+1)\tau+2h], \ldots, \Delta(mk\tau)\}\\ =(&D_1, D_2, \ldots, D_N, D_{N+1}, \ldots, D_{mN}).\end{aligned} \tag{D1}$$

Here ζ is nmN dimensional. The evolution equations are

$$\zeta_1(k+1) = \zeta_{mN}(k) + \{f'[x(mk\tau+\tau_2)]\zeta_{mN}(k) - \epsilon\zeta_{mN-j}(k)\}h,$$

$$\zeta_2(k+1) = \zeta_1(k+1) + \{f'[x(mk\tau+\tau_2+h)]\zeta_1(k+1) - \epsilon\zeta_{mN-j}(k)\}h,$$

$$\vdots$$

$$\zeta_N(k+1) = \zeta_{N-1}(k+1) + (f'\{x[mk\tau+\tau_2+(N-1)h]\} \times \zeta_{N-1}(k+1) - \epsilon\zeta_{mN-j}(k))h,$$

$$\zeta_{N+1}(k+1) = \zeta_N(k+1) + (f'\{x[(mk+1)\tau+\tau_2]\} \times \zeta_N(k+1) - \epsilon\zeta_{(m+1)N-j}(k))h,$$

$$\zeta_{N+2}(k+1) = \zeta_{N+1}(k+1) + (f'\{x[(mk+1)\tau+\tau_2+h]\} \times \zeta_{N+1}(k+1) - \epsilon\zeta_{(m+1)N-j}(k))h,$$

$$\vdots$$

$$\zeta_{iN}(k+1) = \zeta_{iN-1}(k+1) + (f'\{x[(mk+i-1)\tau+\tau_2 + (N-1)h]\}\zeta_{iN-1}(k+1) - \epsilon\zeta_{(m+i-1)N-j}(k))h,$$

$$\zeta_{iN+1}(k+1) = \zeta_{iN}(k+1) + (f'\{x[(mk+i)\tau+\tau_2]\} \times \zeta_{iN}(k+1) - \epsilon\zeta_{(m+i)N-j}(k))h,$$

$$\vdots$$

$$\zeta_{mN}(k+1) = \zeta_{mN-1}(k+1) + (f'\{x[(mk+m-1)\tau+\tau_2 + (N-1)h]\}\zeta_{mN-1}(k+1) - \epsilon\zeta_{(2m-1)N-j}(k))h. \quad \text{(D2)}$$

Each evolution of ζ advances the time by $m\tau$. The transverse Lyapunov exponents are calculated using the standard orthonormalization procedure. The number of transverse Lyapunov exponents that can be calculated is $n+ml$, indication that the dimension of the coupled system is $2n+ml$.

[1] L. M. Pecora and T. L. Carroll, Phys. Rev. A **44**, 2374 (1991).
[2] C. Tresser, P. A. Worfolk, and H. Bess, Chaos **5**, 693 (1995).
[3] R. E. Amritkar and Neelima Gupte, Phys. Rev. E **47**, 3889 (1993).
[4] S. Boccaletti, J. Kurths, G. Osipov, D. L. Valladares, and C. S. Zhou, Phys. Rep. **366**, 1 (2002).
[5] N. J. Corron, J. N. Blakely, and S. D. Pethel, Chaos **15**, 023110 (2005).
[6] K. Pyragas, Phys. Rev. E **58**, 3067 (1998).
[7] S. Zhou, H. Li, and Z. Wu, Phys. Rev. E **75**, 037203 (2007).
[8] M. Y. Choi, H. J. Kim, D. Kim, and H. Hong, Phys. Rev. E **61**, 371 (2000).
[9] M. J. Bunner and W. Just, Phys. Rev. E **58**, R4072 (1998).
[10] M. K. Stephen Yeung and S. H. Strogatz, Phys. Rev. Lett. **82**, 648 (1999).
[11] U. Ernst, K. Pawelzik, and T. Geisel, Phys. Rev. E **57**, 2150 (1998).
[12] E. M. Shahverdiev, S. Sivaprakasam, and K. A. Shore, Phys. Lett. A **292**, 320 (2002).
[13] M. Zhan, X. Wang, X. Gong, G. W. Wei, and C. H. Lai, Phys. Rev. E **68**, 036208 (2003).
[14] S. H. Park, S. Kim, H.-B. Pyo, and S. Lee, Phys. Rev. E **60**, 4962 (1999).
[15] Y. Wang, Z. D. Wang, Y. X. Li, and X. Pei, J. Phys. Soc. Jpn. **72**, 443 (2003).
[16] G. C. Sethia, A. Sen, and F. M. Atay, Phys. Rev. Lett. **100**, 144102 (2008).
[17] Y. Nakamura, F. Tominaga, and T. Munakata, Phys. Rev. E **49**, 4849 (1994).
[18] K. Konishi and H. Kokame, Phys. Lett. A **366**, 585 (2007).
[19] A. Prasad, Phys. Rev. E **72**, 056204 (2005).
[20] D. V. Ramana Reddy, A. Sen, and G. L. Johnston, Phys. Rev. Lett. **80**, 5109 (1998).
[21] H. U. Voss, Phys. Rev. E **61**, 5115 (2000).
[22] H. J. Wang, H. B. Huang, and G. X. Qi, Phys. Rev. E **71**, 015202(R) (2005).
[23] H. U. Voss, Phys. Rev. Lett. **87**, 014102 (2001).
[24] H. J. Wang, H. B. Huang, and G. X. Qi, Phys. Rev. E **72**, 037203 (2005).
[25] M. Ciszak, J. M. Gutiérrez, A. S. Cofino, C. Mirasso, R. Toral, L. Pesquera, and S. Ortin, Phys. Rev. E **72**, 046218 (2005).
[26] T. Heil, I. Fischer, W. Elsässer, J. Mulet, and C. R. Mirasso, Phys. Rev. Lett. **86**, 795 (2001).
[27] S. Tang and J. M. Liu, Phys. Rev. Lett. **90**, 194101 (2003).
[28] R. He and P. G. Vaidya, Phys. Rev. E **57**, 1532 (1998).
[29] Z. Li and D. Xu, Chaos, Solitons Fractals **22**, 477 (2004).
[30] X. Wang, X. Wu, Y. He, and G. Aniwar, Int. J. Mod. Phys. B **22**, 3709 (2008).
[31] P. G. Vaidya and S. Angadi, Chaos, Solitons Fractals **17**, 379 (2003).
[32] K. M. Short and A. T. Parker, Phys. Rev. E **58**, 1159 (1998).
[33] J. H. Peng, E. J. Ding, M. Ding, and W. Yang, Phys. Rev. Lett. **76**, 904 (1996).
[34] V. S. Udaltsov, J. P. Goedgebuer, L. Larger, and W. T. Rhodes, Phys. Rev. Lett. **86**, 1892 (2001).
[35] J. P. Goedgebuer, L. Larger, and H. Porte, Phys. Rev. Lett. **80**, 2249 (1998).
[36] D. Ghosh, S. Banerjee, and A. R. Chowdhury, EPL **80**, 30006 (2007).
[37] L. Yaowen, G. Guangming, Z. Hong, W. Yinghai, and G. Liang, Phys. Rev. E **62**, 7898 (2000).
[38] D. V. Senthilkumar and M. Lakshmanan, Phys. Rev. E **71**, 016211 (2005).
[39] J. Doyne Farmer, Physica D **4**, 366 (1982).
[40] S. Boccaletti, A. Farini, and F. T. Arecchi, Phys. Rev. E **55**, 4979 (1997).